Direct Determination of Energy Dissipation in Stirred Vessels with Two-Point LDA

A. Ducci and M. Yianneskis
Experimental and Computational Laboratory for the Analysis of Turbulence (ECLAT), Department of Mechanical Engineering, King's College London, Strand, London, WC2R 2LS, U.K.

DOI 10.1002/aic.10468
Published online May 19, 2005 in Wiley InterScience (www.interscience.wiley.com).

The ensemble-averaged kinetic energy viscous dissipation rate was determined with a multipoint LDA technique in a vessel stirred by a Rushton turbine. Nine out of the total of 12 mean squared velocity gradients constituting the dissipation rate were directly measured in the impeller stream, and the deviation of the flow from local isotropy was investigated. The dissipation rate normalized with N^3D^2, where N and D are the impeller rotational speed and the impeller diameter, respectively, was found to be approximately constant for Reynolds numbers of 20,000–40,000, whereas the fluctuating gradients were found to vary significantly, by up to three times the ensemble-averaged values, with blade angular position. The ensemble-averaged dissipation rate values were also assessed through a local turbulence kinetic energy balance. © 2005 American Institute of Chemical Engineers *AIChE J,* 51: 2133–2149, 2005
Keywords: turbulence dissipation rate, multipoint LDA, kinetic energy production, phase-resolved dissipation rate, stirred vessels

Introduction

The viscous dissipation rate of turbulent kinetic energy (ε) is a key parameter for mixing in stirred reactors because it influences a wide range of chemical processes, from breakup of drops, particles, bubbles, in liquid–liquid, solid–liquid, and gas–liquid systems, respectively, to crystallization and flocculation. Although values of the average dissipation rate can be readily obtained from the power number, these are insufficient for many practical purposes where the local ε distribution is required. For example, the minimum drop size in a dispersion is determined by the maximum dissipation rate, ε_{max} (see Zhou and Kresta[1]). Other examples are the so-called "bulk flow" and "turbulence" models often used to assess mixing effectiveness for homogenization applications (see Nienow[2]), which depend on reliable ε values being available. Similarly, improved population balance approaches for the modeling of drop distributions in stirred tanks necessitate knowledge of the local distribution of ε in the regions that the flow domain is subdivided into (see Alopaeus et al.[3]), whereas knowledge of the power dissipation relevant to the region of drop dispersion is necessary to analytically estimate drop sizes (see Davies[4]). Pacek et al.[5] concluded that for improved understanding of drop dispersion, local dissipation rates need to be measured for a wide range of impellers. In addition, determination of micromixing in a stirred tank using parallel reactions (see Bourne and Yu[6]) relies on good knowledge of the ε distribution in the tank.

To date different approaches and techniques have been used to determine the magnitude and the distribution of the dissipation rate, especially of its maximum and minimum values, but these have met with limited success, primarily because of the high resolution that the measurements require to fully resolve the energy dissipated in the smallest eddies.

One of the earliest studies of the kinetic energy viscous dissipation rate was performed by Cutter[7] with a photographic method. Starting from the Navier–Stokes equations, Cutter derived Eq. 1 to estimate the average dissipation rate over a volume from the decrease of flux of total kinetic energy

Correspondence concerning this article should be addressed to M. Yianneskis at michael.yianneskis@kcl.ac.uk.

through the surface of an annulus of radius r and width dr and to a term related to the flux of the most significant shear stress $\overline{u_r u_\theta}$.

$$2\pi r \int \varepsilon dz = \frac{\partial}{\partial r}\left[2\pi r \int (K^2 \bar{U}_r + 2\bar{U}_\theta \overline{u_r u_\theta}) dz\right] \quad (1)$$

where K^2 is the sum of all the mean and root mean squared (rms) velocity components squared. Among the different assumptions made to derive Eq. 1 the most restrictive are isotropy of the turbulent fluctuations and the axial mean velocity being negligible over the entire vessel. $\varepsilon/\bar{\varepsilon}$ was found to vary from values of 70 close to the impeller to 4 far from the impeller.

Since then, extensive studies have been carried out and different approaches and approximations have been attempted to estimate the local dissipation rate of turbulent kinetic energy. The experimental approaches can be broadly subdivided into three main methods: (1) those using dimensional methods, (2) a kinetic energy balance, and (3) the direct determination of ε from its definition.

In the first method the local dissipation rate is determined from an equation of the following form

$$\varepsilon = A \frac{u_r'^3}{\Lambda} \quad (2)$$

where A is a constant ($\approx$1), u_r is the rms of the fluctuating velocity component in the radial (main flow) direction, and Λ is the integral length scale generally estimated as 0.1 times the impeller diameter D. To derive Eq. 2 it is necessary to assume isotropic turbulence and a constant integral length scale in the entire vessel. Despite the approximations involved, Kresta and Wood[8] showed that use of Eq. 2 gives very reliable estimates of the local dissipation rate.

To take into account the anisotropy of the flow, Wu and Patterson[9] determined the local dissipation rate through a dimensional method, by replacing the rms of the fluctuating velocity in the radial direction u_r with $\sqrt{0.5q^2}$. They then determined the value of A as being 0.85 by equating the integral of the local dissipation rate estimations over the volume of an annulus to the decrease of flux of kinetic energy over the surface of the annulus. The maximum $\varepsilon/\bar{\varepsilon}$ was found to be 22 and located close to the impeller.

In the second method the local dissipation rate is determined by solving the following kinetic energy balance equation once all other terms have been evaluated

$$\frac{1}{2}\frac{\partial \overline{q^2}}{\partial t} + \underbrace{\frac{1}{2}\bar{U}_i \frac{\partial \overline{q^2}}{\partial x_i}}_{\text{Convection}} = \underbrace{-\overline{u_i u_j}\frac{\partial \bar{U}_i}{\partial x_j}}_{\text{Production}} \underbrace{-\frac{1}{2}\frac{\partial}{\partial x_i}\overline{(u_i q^2)}}_{\text{Turbulent diffusion}} \underbrace{-\frac{\partial}{\partial x_i}\overline{\left(u_i \frac{p}{\rho}\right)}}_{\text{Pressure diffusion}}$$

$$\underbrace{+\nu \frac{\partial}{\partial x_i}\overline{u_j\left(\frac{\partial u_i}{\partial x_j}+\frac{\partial u_j}{\partial x_i}\right)}}_{\text{Viscous diffusion}} \underbrace{-\nu\overline{\frac{\partial u_j}{\partial x_i}\left(\frac{\partial u_i}{\partial x_j}+\frac{\partial u_j}{\partial x_i}\right)}}_{\text{Viscous dissipation}} \quad (3)$$

In this way it is not necessary to resolve the flow down to the smallest dissipative scales, but some assumptions have to be made about terms such as the pressure diffusion that cannot be directly determined with an anemometer. Moreover, the accuracy of the dissipation rate calculated in this way is substantially affected by the individual errors involved in the estimation of each of the terms of Eq. 3. Escudié and Liné[10] carried out PIV experiments in a vessel stirred by a Rushton turbine for a Reynolds number (Re) of 56,200. They decomposed the velocity flow field into mean, periodic, and turbulent motions and, solving separately the energy balance equations for each motion, they were able to estimate the kinetic energy pressure diffusion attributed to the organized motion and the local dissipation rate of the turbulent motion. They found that $\varepsilon/(N^3D^2)$ increased in the radial direction along the centerline of the impeller stream, reaching a maximum of 14 at r/T = 0.23. A comparison with the dissipation rate calculated with the dimensional method showed that the latter overestimates the dissipation in the impeller stream region.

A different dynamic equilibrium approach was used by Sheng et al.,[11] who measured the local dissipation rate in a vessel stirred by a pitched blade turbine for Re = 9200 with a large eddy PIV method and a subgrid-scale (SGS) model. Their approach assumes a dynamic equilibrium between the kinetic energy transferred from largest to smallest scales, allowing the determination of the dissipation rate directly from the flux of turbulent kinetic energy through the inertial subrange. Using this approach they obviated the need for a high resolution PIV capable of resolving the Kolgomorov scales.

In the third method the local dissipation rate of kinetic energy is estimated directly from the definition of ε shown in the following equation (see Hinze[12])

$$\varepsilon = \nu\overline{\left(\frac{\partial u_i}{\partial x_j}+\frac{\partial u_j}{\partial x_i}\right)\frac{\partial u_i}{\partial x_j}} \quad (4)$$

In using this method, one needs to make assumptions of local isotropy for the terms that have not been determined and a high-resolution anemometer is necessary to fully resolve the dissipative scales. Sharp and Adrian[13] used a two-dimensional (2D) PIV system in a vessel stirred by a Rushton turbine to determine the dissipation rate from five out of the total of 12 terms of Eq. 4. They concluded that the use of the isotropy hypothesis can lead to an overestimation of the true dissipation rate. Using a Smagorinsky model they estimated the subgrid-scale dissipation rate and found that the dissipation rate they were able to resolve with the PIV was at least 70% of the total. The maximum of $\varepsilon/\bar{\varepsilon}$ was found to be 15 at a radial position r/T = 0.196. Michelet[14] measured the kinetic energy viscous dissipation rate in a vessel stirred by a Rushton turbine (for Re = 27,000) directly with a two-point laser Doppler anemometer (LDA). The local dissipation rate was estimated in the impeller stream from nine out of the total of 12 terms of Eq. 4, but its integral over the volume of measurement yielded only 6.8% of the total energy input in the vessel, raising some doubts about the resolution of the system.

Although much useful data have been obtained, as a result of the complexity of measuring ε and the approximations made and/or limitations involved in earlier efforts, different estimates of ε can often vary. For example, the amount of energy dissipated in the impeller swept area, the impeller stream and the bulk of the vessel has been estimated by the large eddy simu-

lation (LES) predictions of Derksen and van den Akker[15] to be 18, 22, and 60% of the total ε, respectively. On the other hand, studies by Ng and Yianneskis,[16] Zhou and Kresta,[17] and Michelet[14] showed, respectively, that 57, 66, and 93% of ε is dissipated in the bulk region.

The present work builds on the approach of Michelet,[14] but with considerably improved and sufficiently fine spatial resolution to resolve the dissipative scales, the kinetic energy balance approach of Escudié and Liné[10] but with the dissipation rate directly measured, and the PIV work of Sharp and Adrian[13] but for a much higher Re. The present measurement approach and relevant implications necessary to alleviate shortcomings of earlier similar approaches and to avoid potential experimental limitations are described where necessary in the following text because the accuracy of the measured ε values depend critically on the procedures adopted.

The present approach aims to overcome the limitations and approximations encountered in earlier efforts to determine ε and thus provide a more accurate estimation of the local dissipation rate in the impeller stream measuring directly nine out of the total of 12 terms that constitute ε. The data obtained can be used to assess the deviation from local isotropy of the flow and consequently determine to what extent the hypothesis of local isotropy can affect the estimation of ε. A four-channel LDA with high spatial resolution was used. The measured ensemble-averaged dissipation rate values were thoroughly compared with similar PIV data obtained in an exactly scaled vessel (see Baldi[18]). In addition, further investigations through comparison of ensemble- and phase-averaged quantities were carried out to assess the variation of the measured values with Re and with the blade angular position respectively. Finally, a kinetic energy balance was made to assess the accuracy of the rate of dissipation determined.

Flow Configuration, LDA System, and Measurement Procedure

The measurements were carried out in a vessel of diameter $T = 294$ mm stirred by a six-blade Rushton turbine of diameter $D = T/3$. The geometrical characteristics of the vessel and of the impeller are shown in Figures 1a and 1b. The four equispaced baffles had a width of $T/10$ and a thickness $T/100$. The vessel, filled with distilled water seeded with neutrally buoyant silver-coated 10-μm hollow particles, was made of glass and was positioned inside a trough also filled with water to minimize the distortion of the laser beams caused by the refraction on the cylindrical surface of the vessel. The bottom was made of stainless steel with a 294-mm-diameter glass window designed to allow optical access from the bottom of the vessel and a lid was positioned at a height H equal to T to prevent the entrainment of air bubbles in the flow. The impeller clearance C was set to $T/3$.

Unless directly stated, in the remainder of this paper a cylindrical coordinate system (r, θ, and z) with origin in the center of the base of the vessel will be used. The impeller rotated in a clockwise direction as viewed from above.

As shown on the right-hand side of Figure 1a the dissipation rate was measured in nine points positioned along an axial ($r/T = 0.225$) and a radial profile ($z/T = 0.33$), along the bisector plane between two adjacent baffles. Although in the locations $z/T = 0.35$ and $z/T = 0.367$ of the axial profile all nine of the mean squared velocity gradients $\overline{(\partial u_i/\partial x_j)^2}$ (with i and j being independently r, z, or θ) could be determined, in the remaining locations the gradients $\overline{(\partial u_z/\partial r)^2}$ and $\overline{(\partial u_r/\partial z)^2}$ could not be directly evaluated because of optical access restrictions. All the gradients were estimated as ensemble-averages with the exception of the $\overline{(\partial u_\theta/\partial r)^2}$ gradient, which was also estimated through phase-averaged measurements at the location $r/T = 0.2$ and $z/T = 0.33$.

To calculate the balance of the rate of change of kinetic energy in the nine points where the dissipation rate was evaluated, most of the terms involved in the kinetic energy balance equation were estimated from two sets of velocity data taken in the vertical plane mesh shown in Figure 1a and in the horizontal plane mesh shown in Figure 1b. In both sets of data two velocity components were measured simultaneously in each point of the mesh. In this way it was possible to estimate all the terms that involve correlation of the velocity components U_r and U_θ and the velocity components U_z and U_θ.

The LDA used is a Dantec Ltd. (Moreton, Merseyside, UK) system that is composed of three probes mounted on a transverse that can be moved in three orthogonal directions. One of the probes can measure two velocity components, whereas the others can measure only one each. Considering a Cartesian coordinate system, the arrangements of the probes for the measurements of the gradients $\overline{(\partial u_1/\partial x_1)^2}$, $\overline{(\partial u_1/\partial x_3)^2}$, $\overline{(\partial u_3/\partial x_3)^2}$, and $\overline{(\partial u_3/\partial x_1)^2}$ are shown in Figure 2. The two-channel probe (no. 2) is displaced along the two directions shown. Depending on the gradient of interest, probe 2 can measure either the U_1 or the U_3 velocity component. This probe is used with a lens of 240 mm focal length and the dimensions of the resulting control volume are $0.034 \times 0.034 \times 0.22$ mm^3. Probes 1 and 3 incorporated lenses of focal length 310 or 500 mm, depending on the gradient to be measured. To reduce the observed length of the control volume of probe 1, the light scattered by the seeding particles is collected in side scatter by probe 3 (and vice versa when the gradients of the U_1 velocity component are considered). From geometry considerations, taking into account that the angle in air between the optical axes of the side probes and of the center probe is about 28° [or 16° when the probes were arranged to measure the gradients $\overline{(\partial u_r/\partial x_j)^2}$ and $\overline{(\partial u_\theta/\partial x_j)^2}$ with the beams entering the vessel from the bottom], the length of the probe 1 volume for side scatter was estimated to be 0.20 mm (or 0.36 mm, respectively). The probes were aligned in air using a pinhole of 50 μm. Once in water, to overcome the effect of refraction, it is necessary to adjust the relative position of the three control volumes along the X_2 axis by a known distance. As suggested by Benedict and Gould,[19] a further optimization of the alignment is achieved by computing the spatial correlation coefficient $R_{ii}(0)$ for different relative positions of the probes, until a maximum $R_{ii}(0)$ value is found.

The spatial gradients $\overline{(\partial u_i/\partial x_j)^2}$ are estimated by calculating the function $f_i(\Delta x_j)$ defined by the following equation for the different positions examined around the reference point x_j

$$f_i(\Delta x_j) = \overline{[u_i(x_j, t) - u_i(x_j + \Delta x_j, t)]^2} \tag{5}$$

When computing the coefficient $f_i(\Delta x_j)$, the velocity fluctuations u_i in the two different points of measurement must correspond to particles that cross the two control volumes at the

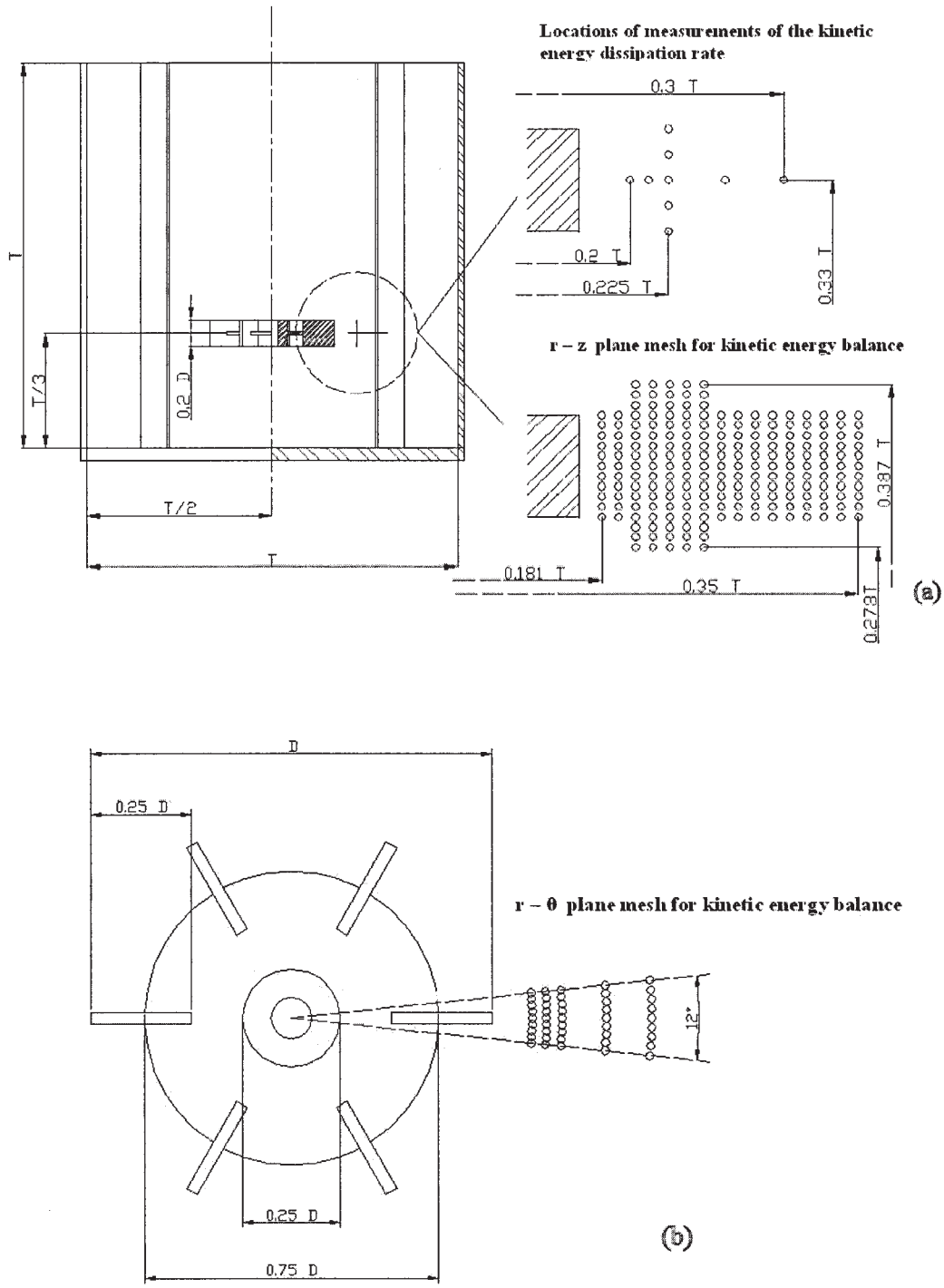

Figure 1. Vessel and impeller used and locations where the measurements were made.

(a) Elevation view; (b) plan view.

same time. This condition is imposed by determining pairs of particles that satisfy the following simultaneity criterion:

$$|t_1 - t_2| < \tau_w$$

where t_1 and t_2 are the arrival times and τ_w is a time coincidence window. In agreement with Kang et al.,[20] the time coincidence window τ_w selected (0.05 ms) is of the order of the transit time taken by the particles to cross the control volume. Using Taylor's hypothesis of frozen turbulence ($U\tau_w$) it is possible to have an estimate of the temporal resolution used to estimate $f_i(\Delta x_j)$ with respect to the local Kolgomorov length scale. The temporal resolution achieved ($\approx 1\eta$) certainly compares very favorably with those used in earlier studies in two-point LDA applications (see, for example, Benedict and Gould[19]).

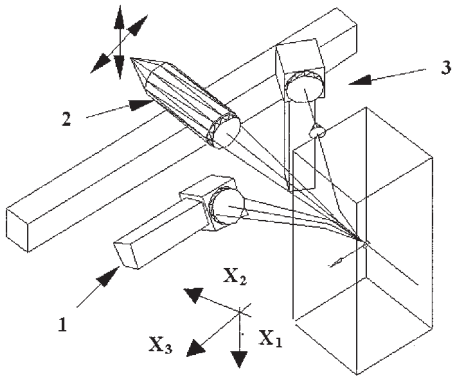

Figure 2. Probe arrangement to measure the velocity gradients $\overline{(\partial u_1/\partial x_1)^2}$, $\overline{(\partial u_1/\partial x_3)^2}$, $\overline{(\partial u_3/\partial x_3)^2}$, $\overline{(\partial u_3/\partial x_1)^2}$.

Once the function $f_i(\Delta x_j)$ is known, the calculation of the spatial gradient can be made from the following expression

$$\overline{\left(\frac{\partial u_i}{\partial x_j}\right)^2} = \lim_{\Delta x_j \Rightarrow 0} \frac{\overline{(u_i(x_j, t) - u_i(x_j + \Delta x_j, t))^2}}{\Delta x_j^2} \tag{6}$$

The spatial gradient can be evaluated by finding the slope of the straight line that best fits the points $[\Delta x_j^2, f_i(\Delta x_j)]$ for Δx_j values close to zero. It should be noted that in the literature the gradients are commonly estimated by interpolating a parabolic curve through the points $[\Delta x_j, R_{ii}(\Delta x_j)]$ and determining the Taylor length scale (see, for example, Benedict and Gould[19]). However, the two procedures were shown to be analogous in the present work, given that the two estimations of the same gradient differed by only 2%. In the rest of the paper the range of points $[\Delta x_j^2, f_i(\Delta x_j)]$, used in the interpolation to estimate the gradient, will be referred to as the fitting range. Before performing the interpolation, it is necessary to identify the range of points $[\Delta x_j^2, f_i(\Delta x_j)]$ around the origin that are affected by single particle–burst-pair bias (see Benedict and Gould[19]). In these points a consistent percentage of the velocity value pairs collected in coincidence arise from single particles that moved sufficiently fast to cross the two control volumes displaced by Δx_j within the time coincidence window. This results in an underestimation of $f_i(\Delta x_j)$ (see Ducci et al.[21]) and a consequent overestimation of the slope, and thus of the gradient, if the points are included in the fitting range. The range of points $[\Delta x_j^2, f_i(\Delta x_j)]$ subjected to this kind of bias can be identified by considering the data rate of the particles in coincidence for different Δx_j. The data rate decreases rapidly as Δx_j increases, until it stabilizes around a constant value above a displacement Δx_{j0}, which is also the first point to be included in the fitting range.

It should be pointed out that the value of Δx_{j0} varies with the mean velocity $\bar{U}_j$ in the direction of the probe displacement and therefore depends on the gradient measured. In the data and figures presented in this work, the points $[\Delta x_j^2, f_i(\Delta x_j)]$ subjected to single particle–burst-pair bias have been removed. It should be noted that the measurement procedure described above has been assessed in a grid-generated turbulent flow, where the dissipation rate of turbulent kinetic energy can be easily calculated from the decay of turbulent kinetic energy along the main flow direction. Moreover, an error analysis aimed at determining the major sources of error in the estimation of the dissipation rate was carried out. In the case of the grid-turbulent flow the errors made in the estimation of a single gradient and of the dissipation rate were found to be 13 and 7%, respectively. The lower error in the estimation of the dissipation rate was justified considering that the errors made in single-gradient measurements tend to average out after the sum shown in Eq. 4.

Preliminary considerations

In previously published works (see Escudié and Liné,[10] Sharp and Adrian,[13] and Michelet[14]), it has been reported that the dissipation rate resulting from the organized motion is only a small percentage of the turbulent dissipation rate (10% for $r/T < 0.2$) and that its value rapidly decreases as the radial distance from the blade increases. Consequently, in the present work the fluctuating velocity component u_i has not been decomposed into periodic and turbulent contributions.

The variation of $f_z(\Delta z)$ with Δz^2 for five different Re values is shown in Figure 3. On the same plot are also shown three curves that represent the variation of $(4\eta)^2$, $(5\eta)^2$, and $(6\eta)^2$ as a function of Re. It must be pointed out that the Kolgomorov scale η was estimated from the value of the local dissipation rate ε, and not from the dissipation rate averaged over the total volume of the vessel ($\bar{\varepsilon}$). As expected, the Kolgomorov scale becomes smaller as Re increases (for example, for Re = 32,000, $\eta = 24$ μm). From Figure 3 it can be seen that the slope of the straight line determined through the fitting procedure described in the previous section depends on the fitting range. As the upper limit of the range ($\Delta z_{\max}$) is decreased, the slope increases and the effect is more significant for higher Re values. On average the percentage differences between the slope calculated within a range of 4η and the ones calculated within ranges of 5 and 6η vary between 10 and 30% respectively. This behavior is expected when the resolution of the measurement is improved and a better estimation of the dissipation in the smallest scales can then be achieved. Gan et al.[22] noted that there is an optimal range of separations of 2–4η for both hot-wire and 2-point LDV measurements that minimize the uncertainty in measuring the gradients. Moreover, Saaren-

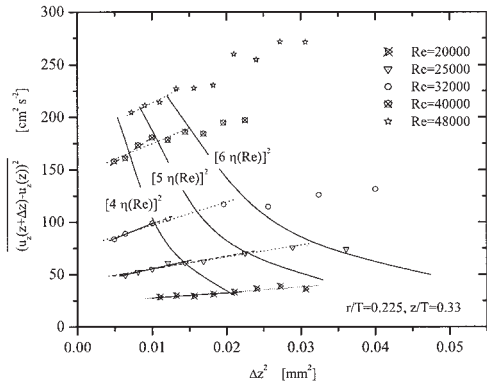

Figure 3. Variation of $\overline{\Delta u_z^2}$ with Δz^2 with Re at $r/T = 0.225$, $z/T = 0.33$.

rinne et al.[23] observed that resolutions of 9 and 2η, respectively, are required to reach 65 and 90% of the true ε value at a point in stirred vessel. The above considerations should explain why Michelet[14] determined very low values of the dissipation rate in the impeller region. Considering that he obtained measurements for Re = 27,000 and that the local Kolgomorov scale η was around 30 μm, the $\Delta x_{j\max}$ of 1.4 mm (47η) that he selected to interpolate the pairs $[\Delta x_j^2, f_i(\Delta x_j)]$ was far too large to resolve the dissipative scales.

The above considerations have led the authors to select a step of 0.01 mm (which is the minimum displacement of the translational stage in use) by which to increment Δx. This ensured that the lower limit of the fitting range Δx_{j0} was determined as accurately as possible and that at least four points were used in the fitting procedure (for most of the gradients determined the $\Delta x_{\max}$ used was 5η). An investigation of the different sources of error, similar to the one carried out for the grid-turbulent flow, has shown that the estimation of the single gradient in the impeller stream is affected by an error of at most 28% (see Ducci[24]). However, as has already been pointed out, the dissipation rate error should be lower.

The effect of Re on the nondimensionalized gradients $\overline{(\partial u_z/\partial z)^2}/(N^3D^2\nu^{-1})$ can be also evaluated from the data shown in Figure 3. Considering the fitting range of 5η, it can be concluded that the gradient $\overline{(\partial u_z/\partial z)^2}/(N^3D^2\nu^{-1})$ does not depend on Re because the values assumed by $\overline{(\partial u_z/\partial z)^2}/(N^3D^2\nu^{-1})$ varied with no particular order around a value of 0.7 with a 10% difference between the maximum and the minimum values obtained. It should be pointed out that the gradient $\overline{(\partial u_z/\partial z)^2}/(N^3D^2\nu^{-1})$ for Re = 48,000 was not included in this estimation because there was only one point $[\Delta z^2, f_z(\Delta z)]$ within the 5η range. Baldi[18] carried out a similar investigation, measuring $\varepsilon/(N^3D^2)$ for different Re values. The $\varepsilon_{\max}/(N^3D^2)$ values increased by 40% as Re decreased from 40,000 to 20,000, assuming a constant value around 10 at the lower end of the Re range. Baldi[18] concluded that the range of variation of $\varepsilon_{\max}/(N^3D^2)$ with Re was a consequence of the lower resolution of the PIV system for the larger Re values, for which the Kolgomorov scales are smaller. For the lower Re cases measured, $\varepsilon_{\max}/(N^3D^2)$ did not vary with Re and Baldi's results are in agreement with those shown herein.

It was therefore decided in the present work to measure all the gradients for Re = 32,000 to ensure both an acceptable resolution and a good data-rate in coincidence.

A different approach to determine ε, using the kinetic energy power spectrum, was also attempted to verify whether the 5η fitting range was sufficient for the resolution of the dissipative scales and to estimate the amount of energy contained above this limit. With this approach, the mean squared velocity gradients $\overline{(\partial u_i/\partial x_i)^2}$ can be estimated through the integral of the energy power spectrum over the wavenumber k_i domain (see Hinze[12])

$$\overline{(\partial u_i/\partial x_i)^2} = \int_0^\infty k_i^2 E_i(k_i)\,dk_i \qquad (7)$$

where E_i is the energy of the u_i velocity component per unit of wavenumber.

It should be pointed out that this approach is based on the frozen turbulence hypothesis, similar to the Taylor hypothesis, because the radial mean velocity is used to move from the frequency domain, after the FFT, to the wavenumber domain.

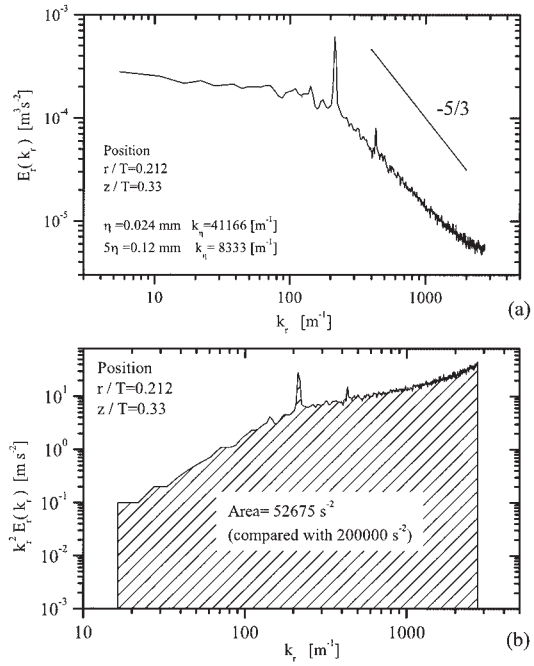

Figure 4. (a) Plot of the energy spectrum of the radial fluctuating component u_r as a function of the radial direction wavenumber k_r in the point (r/T = 0.212; z/T = 0.33). (b) Plot of the power spectrum of the radial fluctuating component u_r as a function of the radial direction wavenumber k_r in the point (r/T = 0.212; z/T = 0.33).

In Figures 4a and 4b the energy spectrum and the power spectrum of the u_r velocity component at $r/T = 0.212$, $z/T = 0.33$ are shown, respectively. From Figure 4a it can be clearly seen that with this approach the data rate of the single-channel LDA was not sufficiently high to resolve the smallest scales of the flow (that is, for the highest wavenumber), given that the maximum wavenumber shown (1200 m^{-1}) is well below that corresponding to 5η (8000 m^{-1}). This is reflected in Figure 4b where the integral of the measured power spectrum (52,675 s^{-2}) corresponds to 25% of the value of the directly measured gradient (200,000 s^{-2}). It should be remarked that the spectrum approach is generally suitable for data obtained with hot-wire anemometers that have a continuous signal and not for data obtained from laser anemometers that have a finite data rate. Consequently, by considering both the spatial and temporal resolutions of the LDA, it was concluded that the most appropriate and accurate manner to determine ε with the LDA is through the direct measurement of the fluctuating velocity gradients using a two-probe arrangement. In addition this approach does not necessitate using Taylor's hypothesis and does not require an extensive use of local isotropy assumptions to estimate ε.

Results

As can be seen from Eq. 4 the expression for the dissipation rate is composed of 12 terms: nine mean squared velocity

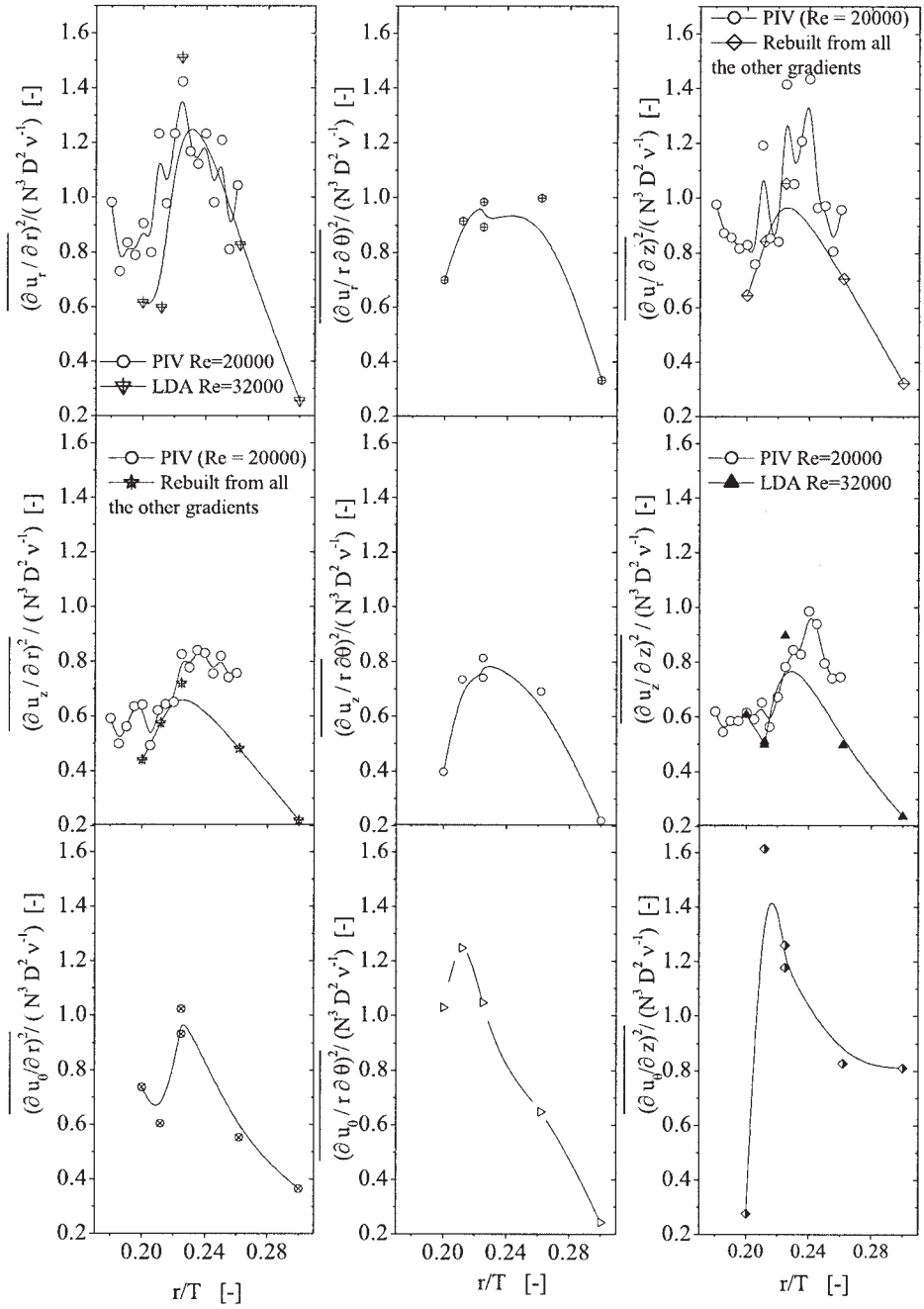

Figure 5. Variation of the nine nondimensionalized mean squared velocity gradients $\overline{(\partial u_i/\partial x_j)^2}$ along the radial profile z/T =0 .33.

gradients $\overline{(\partial u_i/\partial x_j)^2}$ and three cross-product gradients $\overline{(\partial u_i/\partial x_j)(\partial u_j/\partial x_i)}$.

The terms $\overline{(\partial u_i/\partial x_j)^2}$ are analyzed in detail in this section, and the approach used to determine the cross-product terms is subsequently described. The determined values of the kinetic energy dissipation rate and of the integral, micro-, and Kolmogorov length scales of the flow are then analyzed. The effect of the blade phase on the mean squared gradient $\overline{(\partial u_\theta/\partial r)^2}$ is also investigated, whereas in the final part of this section the kinetic energy budget is estimated through a balance of all the terms in Eq. 3.

Mean squared velocity gradients

The variations of the nine nondimensionalized mean squared gradients $\overline{(\partial u_i/\partial x_j)^2}/(N^3D^2\nu^{-1})$ along a radial ($z/T = 0.33$) and an axial ($r/T = 0.225$) profile are shown in Figures 5 and 6, respectively. As already mentioned, the gradients $\overline{(\partial u_z/\partial r)^2}$ and $\overline{(\partial u_r/\partial z)^2}$ were directly measured in only two locations, $z = 0.35T$ and $z = 0.367T$, in the axial profile. For the remaining points the value of $\overline{(\partial u_z/\partial r)^2}$ at a location r/T, z/T was estimated from the other $\overline{(\partial u_i/\partial x_j)^2}$ gradients directly measured in the same location, using the weighted average defined in Eq. 8. The same method was applied to estimate the gradient $\overline{(\partial u_r/\partial z)^2}$.

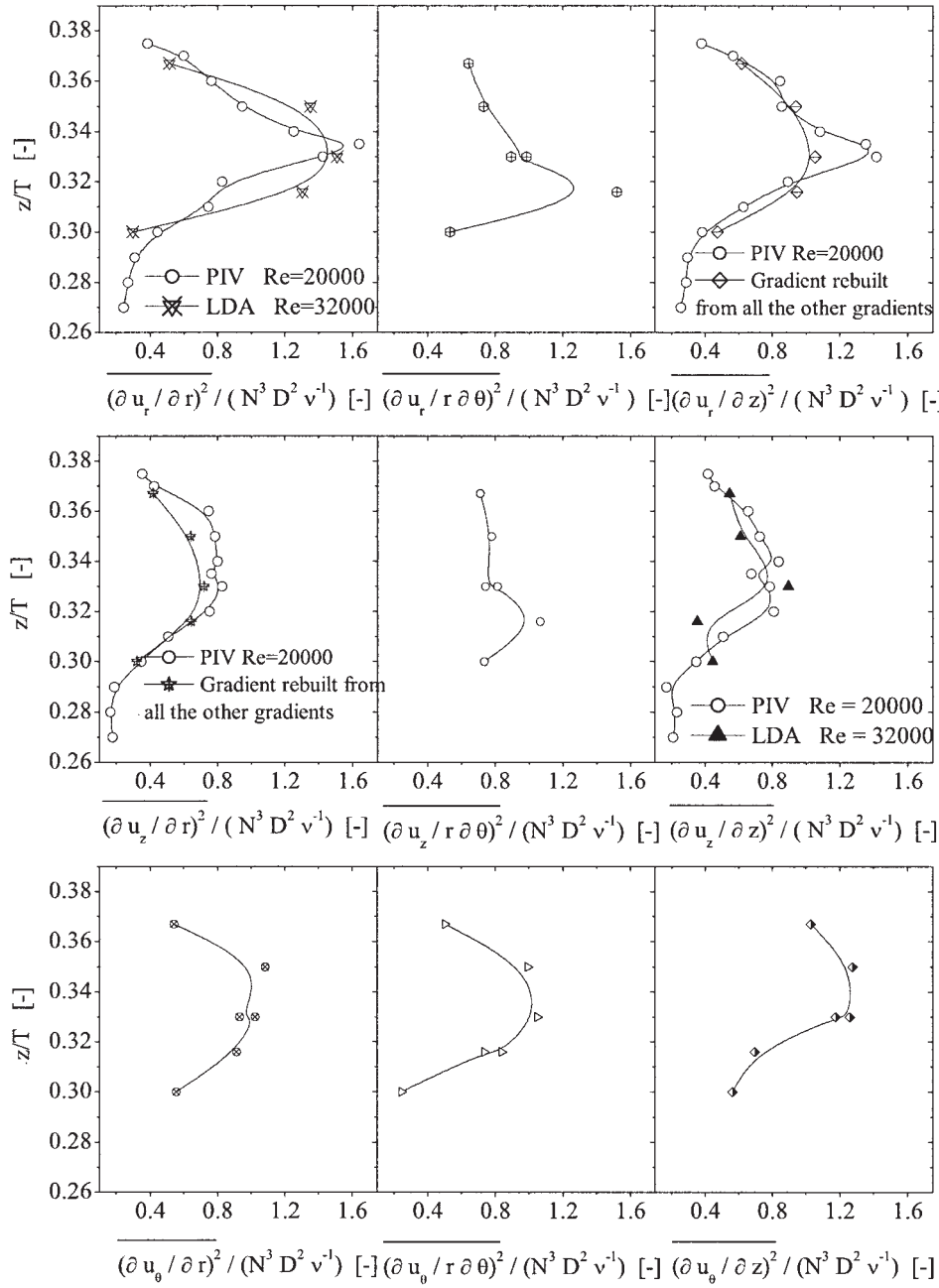

Figure 6. Variation of the nine nondimensionalized mean squared velocity gradients $\overline{(\partial u_i/\partial x_j)^2}$ along the axial profile r/T = 0.225.

$$\left.\overline{\left(\frac{\partial u_z}{\partial r}\right)^2}\right|_{\substack{r/T\\z/T}} = \frac{1}{N}\sum_{i,j}\left[\frac{\left[\overline{\left(\frac{\partial u_z}{\partial r}\right)^2}\Big/\overline{\left(\frac{\partial u_i}{\partial x_j}\right)^2}\right]_{\substack{r/T=0.225\\z/T=0.35}} + \left[\overline{\left(\frac{\partial u_z}{\partial r}\right)^2}\Big/\overline{\left(\frac{\partial u_i}{\partial x_j}\right)^2}\right]_{\substack{r/T=0.225\\z/T=0.367}}}{2}\right]\left.\overline{\left(\frac{\partial u_i}{\partial x_j}\right)^2}\right|_{\substack{r/T\\z/T}} \tag{8}$$

where N is equal to the number, seven, of $\overline{(\partial u_i/\partial x_j)^2}$ evaluated in the point (r/T; z/T).

The radial profiles of the nine mean squared velocity gradients in Figure 5 show that almost all gradients exhibit a significant increase, by around 200%, over a relatively small distance (around $0.2 < r/T < 0.225$), reaching a maximum value at $r/T \approx 0.225$ and thereafter decreasing with increasing distance from the blades. The repeatability of the measurements was extensively assessed, particularly for the gradients $\overline{(\partial u_r/r\partial\theta)^2}$, $\overline{(\partial u_z/r\partial\theta)^2}$, $\overline{(\partial u_\theta/\partial r)^2}$, $\overline{(\partial u_\theta/r\partial\theta)^2}$, and $\overline{(\partial u_\theta/\partial z)^2}$ at $r/T = 0.225$, $z/T = 0.33$. The maximum difference between two repeated measurements was found to be 12.5%. The gradients $\overline{(\partial u_r/\partial r)^2}$, $\overline{(\partial u_z/\partial z)^2}$, $\overline{(\partial u_z/\partial r)^2}$, and $\overline{(\partial u_z/\partial z)^2}$ were compared with the PIV measurements of Baldi,[18] which were carried in a 100-mm vessel at Re = 20,000, and the corresponding PIV data are also shown in Figure 5. Considering the different errors involved in the two sets of measurements, the different Re values, and the small geometrical differences between the two vessels, the agreement is considered to be good, particularly in the region closer to the impeller ($0.2 < r/T < 0.225$).

The axial profiles of the gradients are shown in Figure 6. The maxima are generally found in the upper half of the impeller blade, with a few exceptions [$\overline{(\partial u_r/r\partial\theta)^2}$, $\overline{(\partial u_z/r\partial\theta)^2}$]. The agreement between the LDA and the corresponding PIV measurements is very good in most locations. It should be noted that the gradients that were calculated using Eq. 8 also show in general good agreement with the PIV measurements, except for the peak value, which is lower for the LDA data [such as by 27% for $\overline{(\partial u_r/\partial z)^2_{\max}}$].

The cumulative contribution of the different gradients to the determination of ε along the axial ($r/T = 0.225$) profile is shown in Figure 7a. For convenience of presentation a more compact notation has been used in the figure, replacing $\overline{(\partial u_i/\partial x_j)^2}$ with $\langle u^2_{i,j}\rangle$. The average magnitudes of the nine gradients over the five different measurement locations in the profile are broadly similar. The maximum and minimum contributions are those of the gradients $\overline{(\partial u_\theta/\partial z)^2}$ and $\overline{(\partial u_z/\partial r)^2}$, 14 and 7% of the total ε, respectively. This is even more evident in Figure 7b where the relative contributions of all terms to the total ε value are represented. In general, the gradients of the tangential and radial fluctuating velocities are both greater than 12% of the total ε. The cumulative and relative contributions to ε along the radial profile were similar to those for the axial profile and are not shown for brevity of presentation.

The coefficients K_{ijhk}, representing the ratio between the terms $\overline{(\partial u_i/\partial x_j)(\partial u_h/\partial x_k)}$ and $\overline{(\partial u_r/\partial r)^2}$ are shown for the axial and radial profiles in Figures 7c and 7d, respectively. When the flow is locally isotropic the coefficients K_{ijhk} assume the values summarized in the following three equations (see Hinze[12]),

$$K_{jjjj} = \overline{\left(\frac{\partial u_i}{\partial x_j}\right)^2} \Big/ \overline{\left(\frac{\partial u_r}{\partial r}\right)^2} = 1 \tag{9}$$

$$K_{ijij} = \frac{1}{2}\overline{\left(\frac{\partial u_i}{\partial x_j}\right)^2} \Big/ \overline{\left(\frac{\partial u_r}{\partial r}\right)^2} = 1 \qquad \text{for } i \neq j \tag{10}$$

$$K_{ijji} = -2\overline{\left(\frac{\partial u_i}{\partial x_j}\right)\left(\frac{\partial u_j}{\partial x_i}\right)} \Big/ \overline{\left(\frac{\partial u_r}{\partial r}\right)^2} = 1 \qquad \text{for } i \neq j \tag{11}$$

From both sets of profiles it can be concluded that the flow is highly anisotropic everywhere (with values around 0.25 showing the highest deviation from isotropy). The smallest deviation form local isotropy is found in two regions near the upper and lower tips of the blade (Figure 7c). In addition to the deviation from isotropy of the present ensemble-averaged data, it is worth noting that Sharp and Adrian[13] also investigated the departure of the turbulence from local isotropy from phase-averaged data. In their study the maximum deviation was found to be 80% at an angle of 20° after the blade.

Cross-product gradients

Sharp and Adrian[13] reported that the estimation of the rate of dissipation can vary significantly (by >50%) if different assumptions of local isotropy, axial symmetry, and statistical isotropy are made for the terms of Eq. 4 that could not be measured.

In this study the cross-product terms were determined using two different methods. The first one, used by Sharp and Adrian[13] and Baldi,[18] is based on the hypothesis of statistical isotropy. In this case only the third relation of local isotropy, shown in Eq. 11, is used and the three cross-product terms are determined from the average of the gradients $\overline{(\partial u_i/\partial x_i)^2}$ as in the following equation:

$$2\overline{\left(\frac{\partial u_i}{\partial x_j}\frac{\partial u_j}{\partial x_i}\right)} = -\frac{\overline{(\partial u_1/\partial x_1)^2} + \overline{(\partial u_2/\partial x_2)^2} + \overline{(\partial u_3/\partial x_3)^2}}{3} \tag{12}$$

Using this approximation the kinetic energy viscous dissipation rate can be directly computed from the sum of the mean squared velocity gradients that were measured in the present study. This method was used for the kinetic energy viscous dissipation rate presented earlier in Figure 7a.

The second method involves determining the three cross-product terms using all local isotropic relations and all the gradients that have been directly measured. In this case the cross-product term is determined from the following expression:

$$2\overline{\left(\frac{\partial u_j}{\partial x_i}\frac{\partial u_i}{\partial x_j}\right)} = -\frac{1}{9}\left\{\sum_{i=1}^{3}\overline{\left(\frac{\partial u_i}{\partial x_i}\right)^2} + 0.5\left[\overline{\left(\frac{\partial u_z}{\partial r}\right)^2} + \overline{\left(\frac{\partial u_z}{r\partial\theta}\right)^2} + \overline{\left(\frac{\partial u_\theta}{\partial r}\right)^2} + \overline{\left(\frac{\partial u_\theta}{\partial z}\right)^2} + \overline{\left(\frac{\partial u_r}{r\partial\theta}\right)^2} + \overline{\left(\frac{\partial u_r}{\partial z}\right)^2}\right]\right\} \tag{13}$$

The difference between the estimates obtained with the two methods and the cross-product term $\overline{(\partial u_r/\partial z)(\partial u_z/\partial r)}$, determined directly from the PIV data of Baldi,[18] is shown in Figures 8a and 8b for the axial and radial profiles, respectively. It is evident that both methods substantially underestimate the true value of $\overline{(\partial u_r/\partial z)(\partial u_z/\partial r)}$. For this reason a third method has been adopted in the calculation of ε, which makes use of the results obtained from the PIV data for Re = 20,000. As already discussed, Re does not have any major effect on the nondimensionalized mean squared gradients constituting the dissipation rate. Consequently, the cross-product terms $\overline{(\partial u_r/\partial z)(\partial u_z/\partial r)}/(N^3D^2\nu^{-1})$ and $\overline{(\partial u_\theta/\partial z)(\partial u_z/r\partial\theta)}/(N^3D^2\nu^{-1})$,

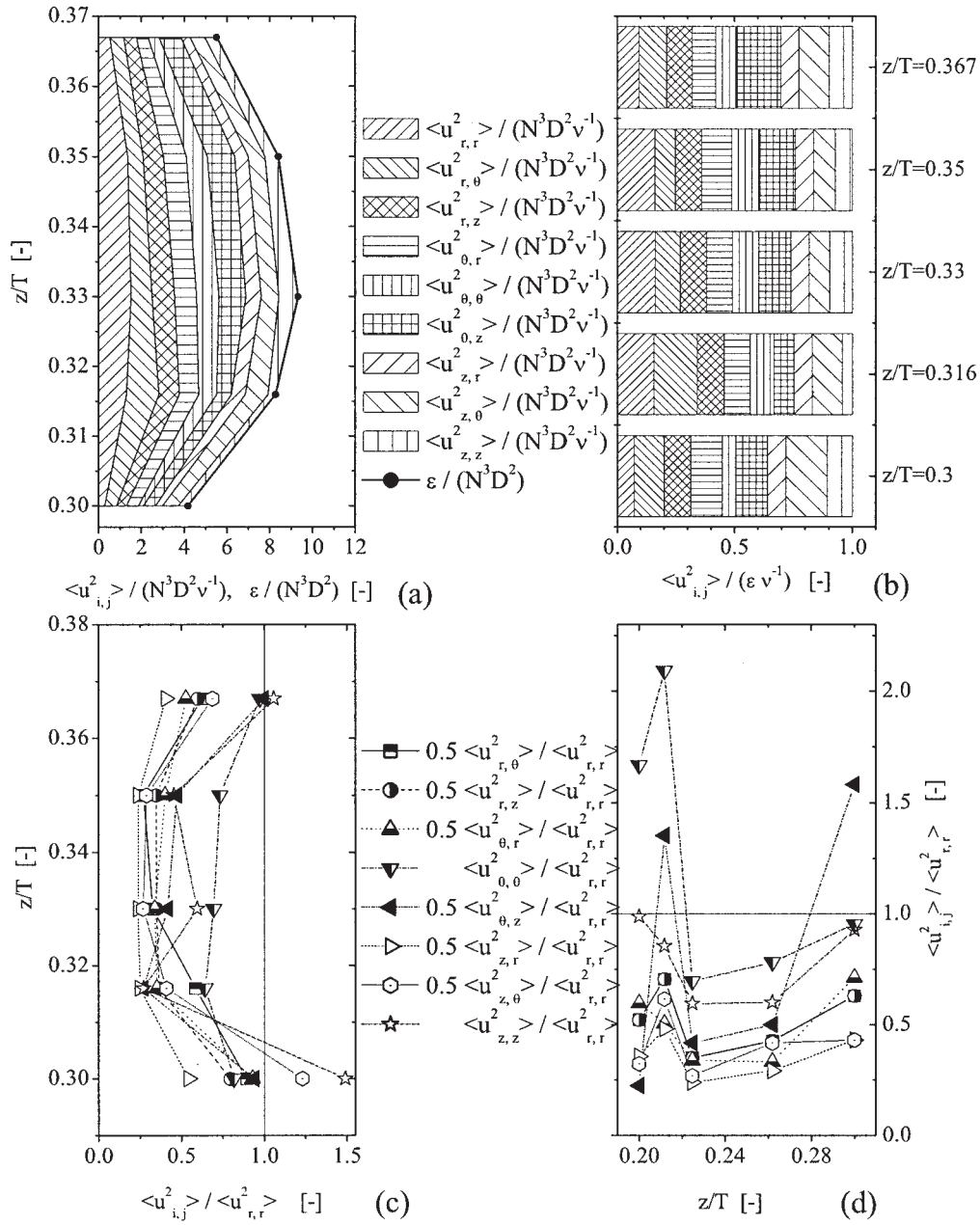

Figure 7. Cumulative (a) and relative (b) contributions to the total kinetic energy viscous dissipation rate of the nine mean squared velocity gradients $\langle u_{i,j}^2 \rangle$ for the axial profile r/T = 0.225; (c) axial (r/T = 0.225) and radial (d) (z/T = 0.33) profiles of the coefficients K_{ijhk}.

which should exhibit a similar trend in the axial and radial profiles, as the derivatives $\partial u_r/\partial z$ and $\partial u_\theta/\partial z$ are similar, were set equal to the nondimensionalized value of $(\partial u_r/\partial z)(\partial u_z/\partial r)/(N^3D^2\nu^{-1})$ measured with PIV. The third cross-product $(\partial u_\theta/\partial r)(\partial u_r/r\partial\theta)$, which was not available from PIV data, was estimated using the second method mentioned above.

Kinetic energy viscous dissipation rate

The effect of the different approximations described in the previous section to determine the terms $(\partial u_i/\partial x_j)(\partial u_j/\partial x_i)$ on the calculation of ε is shown in Figures 9a and 9b for the radial and axial profiles, respectively. The maximum of the dissipation rate calculated with the first method (that is, using the assumption of statistical isotropy) is 30% smaller than the maximum of the dissipation rate calculated through the third method (that is, using both LDA and PIV data). These two curves can be considered as the upper and lower bounds of the true value of the dissipation rate. From Figure 9 it can be observed that the dissipation rate directly calculated by Baldi[18] from PIV data with the assumption of statistical isotropy is contained within the range of values obtained by the first and third methods and matches well with the dissipation rate estimated from the LDA data using the same approximation (the first method).

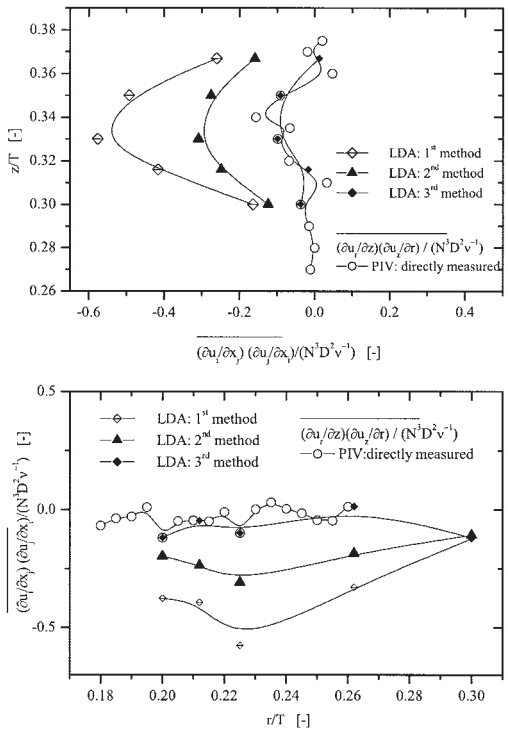

Figure 8. Variation of the nondimensionalized cross-product gradients $\overline{(\partial u_i/\partial x_j)(\partial u_j/\partial x_i)}$ estimated using different methods for (a) the axial r/T = 0.225 and (b) the radial z/T = 0.33 profiles, respectively.

This is not the case for the nondimensionalized dissipation rate calculated with the dimensional method (also shown in Figure 9) by using Eq. 2. It can be clearly seen from both the axial and radial profiles that the dimensional method underestimates the dissipation rate everywhere, except for a region close to the impeller ($r/T = 0.19$), where it exhibits a local maximum (Figure 9a). The maximum is found nearer the impeller in comparison to the position of the maxima ($r/T = 0.225$) obtained from both the LDA and the PIV results. Sheng et al.[11] also found, for a pitched-blade turbine, that the average ε in the impeller region is underestimated by the dimensional method. It should be noted that Zhou and Kresta[1] found a maximum dissipation $\varepsilon_{max}/(N^3D^2)$ of 12 at Re of 31,000 using the dimensional method, which is in close agreement with values directly measured in this work. However, the value of 12 is different from that (maximum $\sim$ 8) calculated with the dimensional method in the present work. It must be emphasized though that the thickness of the blade of the impeller (and therefore the power input) used by Zhou and Kresta[1] was not specified, so exact quantitative comparisons cannot be made.

Turbulence length scales

The Kolgomorov scales were evaluated from the kinetic energy viscous dissipation rate using the following equation:

$$\eta = \left(\frac{\nu^3}{\varepsilon}\right)^{0.25} \tag{14}$$

The variations of the Kolgomorov length scale along the axial and radial profiles are shown in Figures 10a and 10b, respectively. The Kolgomorov scale assumes the lowest value of 23.5 μm in the position where the dissipation rate reaches a maximum. Over the remainder of the two profiles, η increases to values of around 30 μm.

The Taylor microlength scale was also calculated, from the following equation:

$$\frac{1}{\lambda_{ij}^2} = \frac{1}{2\overline{u^2}}\overline{\left(\frac{\partial u_i}{\partial x_j}\right)^2} \tag{15}$$

For brevity, only the Taylor microlength scales λ_{ij} calculated in the point ($r/T = 0.225$; $z/T = 0.33$) are shown in Figure 11a. The λ_{ij} values are all very similar, around 0.62 mm.

The integral length scale Λ_{ij} was calculated from its definition (Eq. 16) by calculating the integral under the curve fitting the spatial correlation coefficients $R_{ii}(\Delta x_j)$ directly measured, as shown in Figure 11b.

$$\Lambda_{ij} = 0.5 \int_{-\infty}^{\infty} R_{ii}(\Delta x_j) d\Delta x_j \tag{16}$$

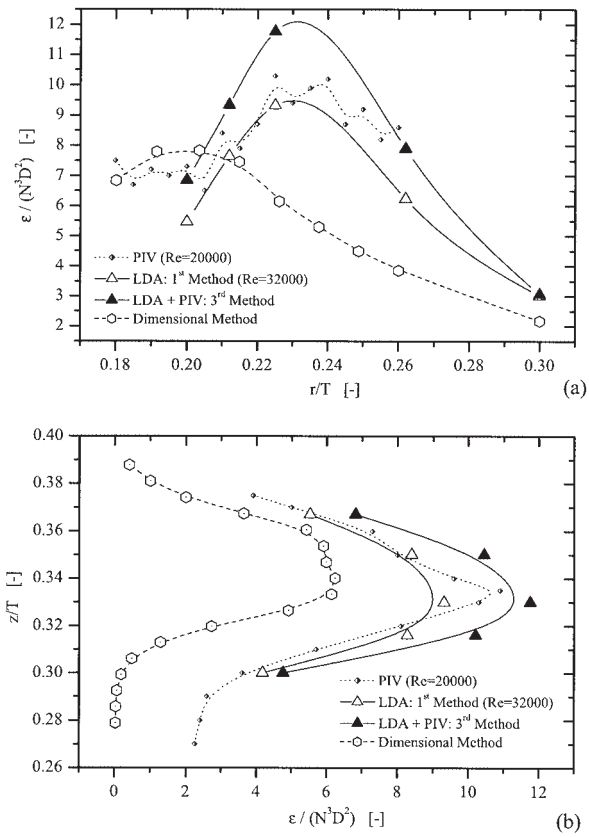

Figure 9. Comparison of the kinetic energy viscous dissipation rate ε calculated from direct measurements using LDA and PIV with the estimates obtained from the dimensional method.

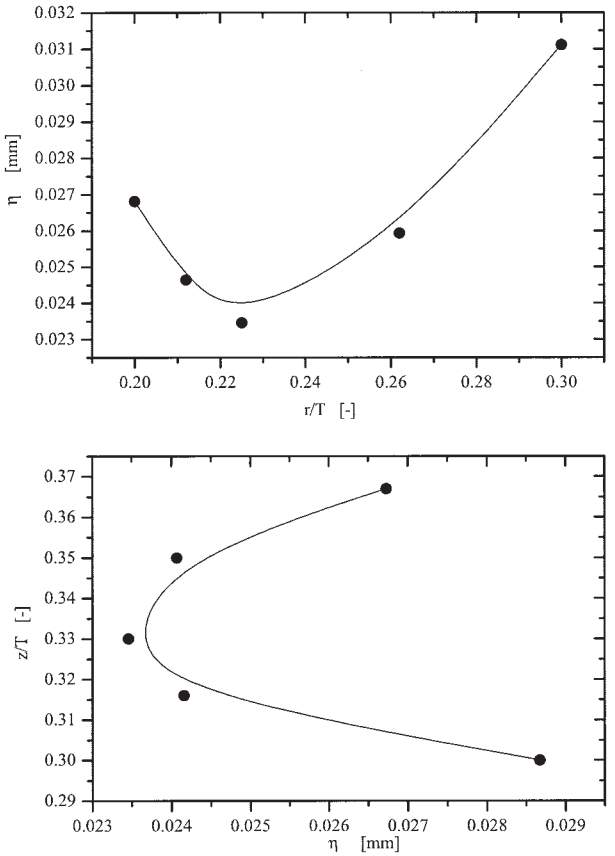

Figure 10. Variation of the Kolgomorov scale along the radial (a) and the axial (b) profiles, respectively.

The integral scales estimated ($\Lambda_{\theta\theta}$, $\Lambda_{\theta z}$, $\Lambda_{\theta r}$, $\Lambda_{r\theta}$, Λ_{rr}) are shown in Figure 11a for the point ($r/T = 0.225$; $z/T = 0.33$). Their values vary between a maximum of 6.2 mm and a minimum of 4 mm for the scales $\Lambda_{\theta\theta}$ and $\Lambda_{\theta z}$, respectively. This is expected, considering the flow in the vessel, given that ensemble averaged-quantities in the tangential direction should vary less than those in the axial direction. The average length scale is 0.046 times the impeller diameter D. Thus the often used value of $0.1D$ may tend to overestimate the integral length scale in the impeller discharge stream and consequently to underestimate the viscous kinetic energy dissipation rate calculated with the dimensional method (as shown in the previous section). This is in agreement with the findings of earlier works where integral length scales in the impeller discharge stream as small as $0.02D$, $0.05D$, and $0.028D$ were previously obtained by Lee and Yianneskis,[25] Wu and Patterson,[9] and Cutter,[7] respectively. Escudié and Liné[10] obtained average Λ values of $0.1D$, but also reported macrostructure varying from $0.01D$ to $0.03D$ close to the blade. It should be noted that replacing the value of $0.1D$ generally used for Λ in Eq. 2 with the value of $0.046D$ should facilitate an estimation of the kinetic energy viscous dissipation rate closer to the values measured directly.

The average integral length scale value of around $0.05D$ may also be considered more appropriate from a consideration of the flow structure close to the blade. The two trailing vortices one above and one below the impeller disk, have diameters smaller than the half height of the blade $0.1D$, near the blade.[26] reported the diameter at $r/T = 0.193$ to be 4.41 mm (that is, $0.045D$) and consequently the ensemble average integral length scale might reasonably be expected to be similar or slightly larger, around $0.05D$. It should be also noted that Khan et al.[27] made similar observations about the integral length scale values near a pitched-blade turbine and also concluded that the often used value of $0.1D$ may be an overestimate close to the impeller and an underestimate away from the blades.

Phase-averaged results

The results presented so far were obtained as ensemble averages over 360° degrees of impeller revolution. However, it is well known that turbulence properties at a location vary substantially with blade angle φ (see, for example, Yianneskis and Whitelaw[28]). In addition, the velocity data contributing to LDA ensemble averages are not evenly distributed among all blades angles (see Lee[29]). However, the low data rates encountered when narrow coincidence windows are necessarily used for fluctuating velocity gradient measurements make phase-resolved measurements very time consuming. In addition, the present measurements were obtained as ensemble averages because they were intended to provide a necessary first stage in the direct determination of ε and to allow comparisons with earlier works. An assessment of both the variation of the gradients with the phase/blade angle and of the effect of the

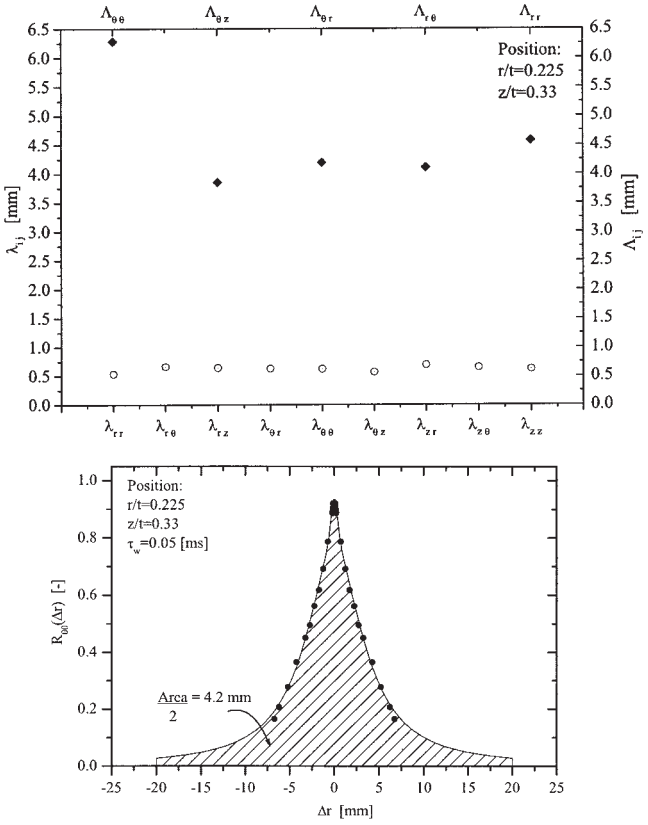

Figure 11. (a) Taylor microscale λ_{ij} and integral length scale Λ_{ij} at r/T = 0.225, z/T = 0.33. (b) Variation of the correlation coefficient $R_{\theta\theta}(\Delta r)$ against Δr at r/T =0.225, z/T = 0.33.

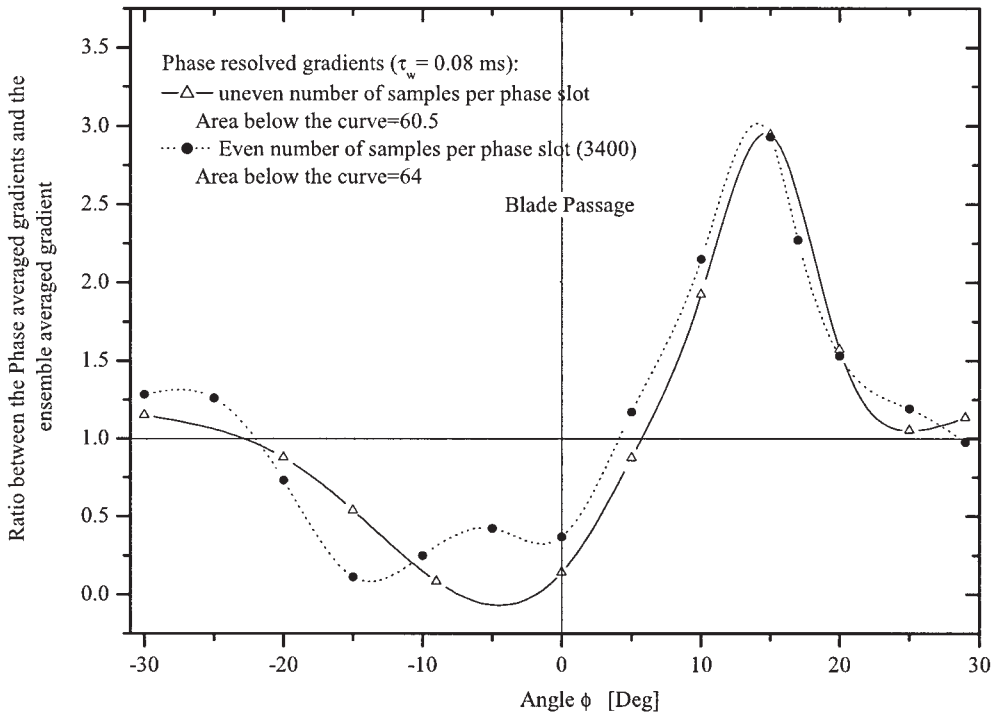

Figure 12. Variation with the phase angle φ of the phase averaged gradient $\overline{(\partial u_\theta/\partial r)^2}\,|_\varphi$ normalized with the ensemble averaged gradient $\overline{(\partial u_\theta/\partial r)^2}$ in the point (r/T = 0.2; z/T = 0.33).

nonuniform number of data from different φ values, however, was considered necessary to indicate the magnitude of such effects.

To estimate the variation of the maximum of the kinetic energy viscous dissipation rate with φ, phase-resolved measurements of the mean squared velocity gradient $\overline{(\partial u_\theta/\partial r)^2}$ were made at $r/T = 0.2$, $z/T = 0.33$. Previous works (for example, Lee and Yianneskis[25]) have shown that the phase-resolved turbulent kinetic energy is highest for $15° < \varphi < 30°$. Consequently a similar behavior might be expected for the kinetic energy viscous dissipation rate. The variation of the phase-resolved $\overline{(\partial u_\theta/\partial r)^2}$ gradient normalized with the correspondingly ensemble-averaged value with the blade/phase angle φ is shown in Figure 12. Two sets of results are shown in the figure. The continuous line indicates the phase-resolved data contributing to ensemble averages such as those reported herein, that is, with uneven numbers of samples from each phase slot. It can be seen that the ratio reaches a very pronounced maximum of 3 at $\varphi = 15°$, whereas values close to 1 are found at 5 and 25–30° after and at 20–30° before the blade. Just before the blade at $\varphi = -10°$, the gradient value is near zero. The φ location of the maximum in the gradient value shown, albeit indicating the contribution of a single term in the ε equation, is in agreement with the phase-resolved ε maxima reported in the LES predictions for a nearly identical vessel by Derksen and van den Akker[15] and by Yeoh,[30] in which the ε maxima were found at $3° < \varphi < 13°$ and $15° < \varphi < 30°$, respectively.

The second set of data (dotted line) shown in Figure 12 corresponds to phase-resolved values that have been obtained with an even number of data (3400) contributing to each phase slot. Accordingly, in this case the value of the ensemble-averaged gradient used in the normalization was calculated from all sets of the even number of data contributing to each phase slot. It can be seen that, although there are small differences with the uneven number of data per phase slot results, the two curves are very similar and the maxima are almost identical. The integral below the two curves shown in Figure 12 provides the total energy dissipated by the term $\overline{(\partial u_\theta/\partial r)^2}$ in the period of time spent between two consequent blade passages. As should be expected the two values, 60 and 64.5 for the uneven and even number of data curves, respectively, differ by less than 7% from the value of 60, that is, of the total energy dissipated by the ensemble-averaged gradient in the same period of time. Consequently, phase-angle bias on the number of samples might be expected to have only a negligible effect on the phase-resolved values. However, the large variation of the $\overline{(\partial u_\theta/\partial r)^2}$ with φ (and consequently of ε with φ) should be kept in mind and quantified in future work.

Kinetic energy balance

The measurements obtained enabled the direct determination of almost all the terms of Eq. 4 constituting convection, turbulent diffusion, production, viscous diffusion, and viscous dissipation rate of kinetic energy for a radial profile at $z/T = 0.33$ and an axial profile at $r/T = 0.225$. A detailed analysis of all measured terms in Eq. 4 is given elsewhere (see Ducci[24]). For brevity of presentation in this section only the production terms are considered in detail but it should be mentioned that the remaining terms of Eq. 4 that were measured were extensively compared with the findings of Escudié and Liné[10] and, notwithstanding the different Re and blade thickness used in

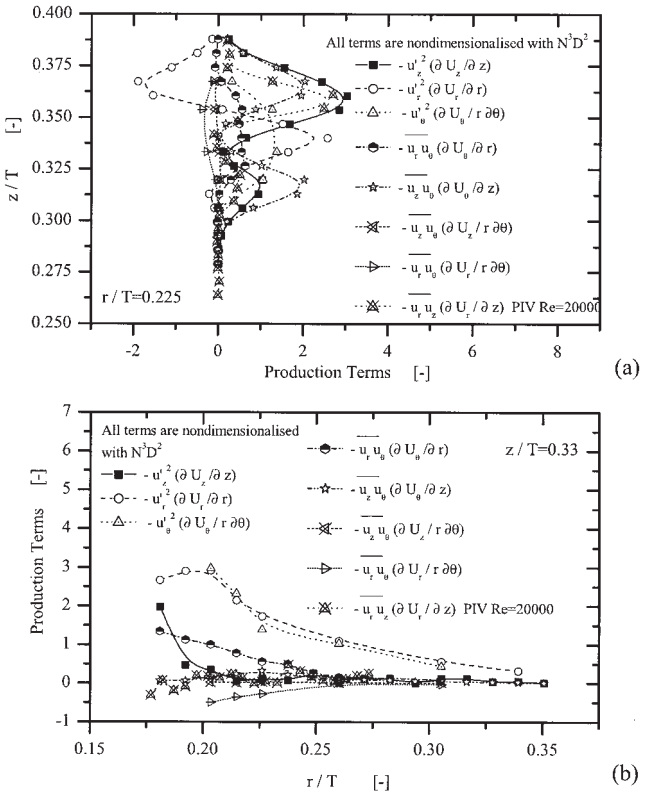

Figure 13. (a) Axial profiles ($r/T = 0.225$) of the seven terms of the kinetic energy production terms evaluated. (b) Radial profiles ($z/T = 0.33$) of the three kinetic energy convective terms.

that work, good qualitative agreement was obtained between the two experiments.

Out of the nine terms constituting the production of kinetic energy, seven were evaluated from the LDA data; their axial and radial profiles are shown in Figures 13a and 13b, respectively. Considering the radial profile of the production terms (Figure 13b), it is evident that the strongest contribution to the production of turbulence along the impeller stream centerline is that arising from the normal Reynolds stresses $\overline{u_r^2}$ and $\overline{u_\theta^2}$. Although for the radial component this is expected, because the mean velocity is decreasing, thus providing energy to the turbulent and organized motions as the fluid moves away from the blade, this trend might not be expected for the tangential term. All the derivatives of ensemble-averaged quantities should be zero in the tangential direction, given that ensemble-averaged data are used. A possible explanation for this behavior may be the small eccentricity of the impeller, of ± 0.5 mm, resulting in a corresponding small displacement Δr of the blade over an arc $r\Delta\theta$. The gradients of the tangential mean velocity in the tangential direction are small, but the described effect is amplified in the production term after the multiplication with the normal stress $\overline{u_\theta^2}$. It should be mentioned that Escudié[31] also reported a nonzero production term $-\overline{u_\theta^2}\partial\overline{U_\theta}/r\partial\theta$. All other terms are smaller and very close to zero along the centerline, except for $-\overline{u_r u_\theta}\partial\overline{U_\theta}/\partial r$.

In the axial profile (Figure 13a), the production term attributed to the normal Reynolds stress of the radial fluctuations, $-\overline{u_r^2}\partial\overline{U_r}/\partial r$, assumes first positive and then negative values with increasing z/T. This can be explained by considering that, on the one hand, the radial mean flow is slowing down along the centerline of the blade, whereas, on the other hand, it is accelerating for $z/T > 0.36$, thus retrieving some of the kinetic energy released to the turbulent and the organized motions. The production term arising from the normal Reynolds stress in the axial direction, $-\overline{u_z^2}\partial\overline{U_z}/\partial z$, assumes values close to zero along the centerline of the blade because in this region the axial mean velocity profile exhibited a plateau of near-zero velocity that separated the lower loop, with positive velocity values below the impeller, from the upper loop with negative velocity values above the impeller. The Reynolds shear stresses $\overline{u_\theta u_z}$ are near-zero along the centerline of the blade with finite values of opposite sign on either side of it. This results in a significant production in the upper and lower parts of the impeller region where the gradients of the tangential velocity in the axial direction assume first positive and then negative values with increasing z/T.

The kinetic energy production term $-\overline{u_r u_\theta}\partial\overline{U_\theta}/\partial r$ is almost constant in the impeller region. Its value is less significant than that of $-\overline{u_z u_\theta}\partial\overline{U_\theta}/\partial z$ because the gradients of mean velocities in the axial direction are greater than those in the radial one. The two terms that could not be evaluated through the LDA data are $(-\overline{u_r u_z}\partial\overline{U_r}/\partial z)$ and $(-\overline{u_r u_z}\partial\overline{U_z}/\partial r)$. From these two terms, the first one should be more significant, given that the gradient of the axial mean velocity in the radial direction is small, especially along the centerline where this component is always very close to zero. The axial profile of $(-\overline{u_r u_z}\partial\overline{U_r}/\partial z)$ should be very similar in shape to that of $(-\overline{u_\theta u_z}\partial\overline{U_\theta}/\partial z)$. In both cases the axial profiles of the radial and tangential velocities are similar, resulting in axial derivatives of same sign across the impeller region and, as shown by Derksen et al.,[32] the shear stresses $\overline{u_r u_z}$ and $\overline{u_\theta u_z}$ also have an analogous asymmetric distribution above and below the blade centerline. It should be noted though that the maximum of $\overline{u_r u_z}$ is 1.5 times greater than $\overline{u_\theta u_z}$. The aforementioned considerations are well matched by the normalized production term $-\overline{u_r u_z}\partial\overline{U_r}/\partial z$ determined through PIV measurements for Re = 20,000 (see Baldi[18]), which is also shown in Figures 14a and 14b. Therefore these results of Baldi have been used when all terms of Eq. 3 were used to obtain a balance of the kinetic energy.

For an incompressible fluid, Eq. 3 can be simplified as follows (see Hinze[12])

$$\frac{1}{2}\frac{\partial\overline{q^2}}{\partial t} + \underbrace{\frac{1}{2}\overline{U_i}\frac{\partial\overline{q^2}}{\partial x_i}}_{\text{Convection}} = \underbrace{-\overline{u_i u_j}\frac{\partial\bar{U}_i}{\partial x_j}}_{\text{Production}} - \underbrace{\frac{1}{2}\frac{\partial}{\partial x_i}\left(\overline{u_i q^2}\right)}_{\text{Turbulent diffusion}} - \underbrace{\frac{\partial}{\partial x_i}\left(\overline{u_i\frac{p}{\rho}}\right)}_{\text{Pressure diffusion}} + \underbrace{\frac{1}{2}\nu\frac{\partial^2\overline{q^2}}{\partial x_i^2}}_{1} - \underbrace{\nu\overline{\left(\frac{\partial u_j}{\partial x_i}\right)^2}}_{2} \tag{17}$$

It must be noted that the last two terms do not represent the viscous diffusion and the viscous dissipation rate in the same manner as in Eq. 3. Nevertheless, use of Eq. 17 considerably simplifies the calculation of the remaining part of the viscous diffusion (the term denoted as 1 which was found to be negligible) and permits the evaluation of the residual part of the viscous dissipation rate, the term denoted as 2, using only the

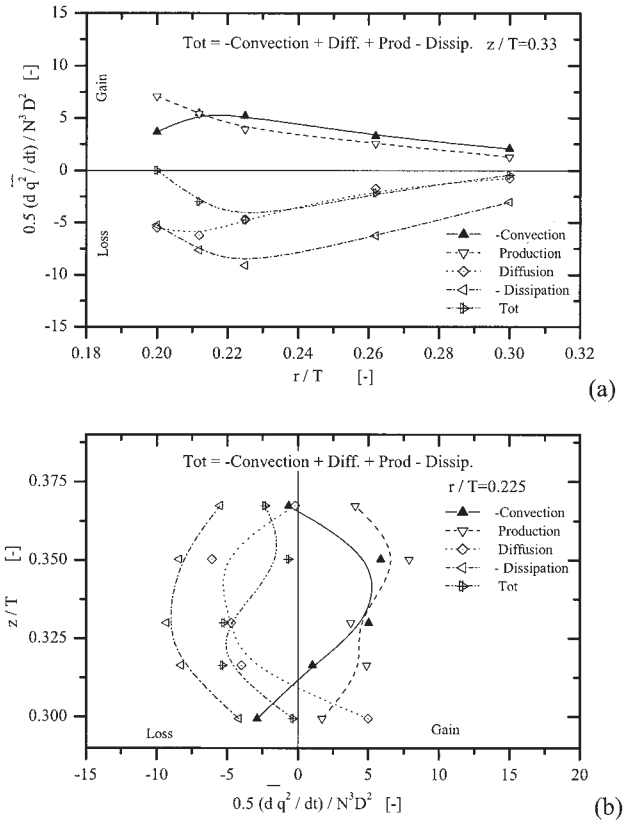

Figure 14. (a) Kinetic energy balance for a profile in the radial direction $z/T = 0.33$. (b) Kinetic energy balance for a profile in the axial direction $r/T = 0.225$.

mean squared velocity gradients that were directly measured with the LDA.

In Figure 14 the balance between the different terms of Eq. 17 is presented. From both Figures 14a and 14b it is possible to note that the convection term has in most locations a positive value because particles traveling toward the wall of the vessel tend to release their kinetic energy in the region as they cross through it. On the contrary, the diffusive term is mostly negative because the kinetic energy tends to diffuse from positions along the centerline of the blade toward the zones closer to the tips of the blade.

The total balance value is mostly negative with a minimum of -5 and an average around -2, whereas the contributing terms vary in magnitude from -10 to $+7.5$. The finite value of the balance may be mainly attributed to the pressure diffusion of the organized motion that could not be determined from the present data. A detailed analysis of the results of Escudié[31] has shown that the axial profiles of the pressure diffusion vary significantly along the radial direction. For a radial position very close to the impeller ($r/T = 0.178$) Escudié's data exhibit two high positive peaks in the regions corresponding to the tips of the blade and an almost zero value on the centerline, whereas for a position $r/T = 0.2$ the axial profile has a maximum on the centerline and decays rapidly as z/T increases or decreases. This behavior reflects qualitatively the trend shown by the total balance of the axial and radial profiles of the present work. Moreover taking into account the difference in Re of the present flow and that of Escudié,[31] the pressure diffusion for $r/T = 0.225$ should have a peak value on the centerline of around 4.5, which should cancel out the negative values found for the total energy balance. Other possible but less significant reasons for the finite balance value include the positional errors involved in the different sets of measurements and the fact that some terms were obtained from PIV data acquired in a smaller vessel with a lower Re, as well as the approximations involved in the use of ensemble-averaged data. Notwithstanding the complexity of measurements of the different terms, the energy balance obtained is very encouraging.

Conclusions

Nine out the total of 12 terms comprising the viscous dissipation rate of kinetic energy of turbulence were directly measured in a vessel stirred by a Rushton turbine through a high-resolution four-channel LDA system. A main objective of the work was to provide a more accurate determination of the maximum value assumed by the nondimensional dissipation rate in the impeller stream region than has been hitherto reported. Other objectives were the evaluation of the effect of Re and of the blade angular position on the ensemble-averaged value of the ε and the fluctuating gradient maxima measured. The ensemble-average value of $\varepsilon_{max}/(N^3D^2)$ was found to be 12 and to be located in the impeller stream centerline at $r/T = 0.225$. Measurements of one of the normalized fluctuating velocity gradients, $\overline{(\partial u_z/\partial z)^2}/(N^3D^2\nu^{-1})$, for $20{,}000 < \mathrm{Re} < 40{,}000$ showed that its value was constant with Re, within 10%, provided that the measurement resolution is around $4-5\eta$. Phase-resolved measurements of the $\overline{(\partial u_\theta/\partial r)^2}$ gradient indicated that its value can vary from 0 to 3 times the ensemble-averaged value, with the maximum found at 15° after the blade. The measurements also allow the assessment of different ways of calculating ε from direct measurements as well as from dimensional relations.

Extensive comparisons of the nondimensional gradients $\overline{(\partial u_i/\partial x_j)^2}/(N^3D^2\nu^{-1})$ and the nondimensional dissipation rate $\varepsilon/(N^3D^2)$ have been made with 2D PIV results. Under similar assumptions of statistical isotropy, the agreement found between the $\varepsilon/(N^3D^2)$ determined with the two techniques was good (10–30% difference). The maximum of $\varepsilon/(N^3D^2)$ was found to vary by at least 30%, depending on the number of terms directly measured because the assumption of statistical isotropy tends to overestimate the absolute value of the cross-product gradients $\overline{(\partial u_i/\partial x_j)(\partial u_j/\partial x_i)}$. Considering the variations of the coefficients K_{ijhk} along the two profiles (the axial profile $z/T = 0.225$ and the radial profile $r/T = 0.33$) where the measurements were carried, the flow was found to deviate significantly (by up to 80%) from local isotropy conditions. As a consequence, dimensional methods, based on the assumption of isotropic flow, may underestimate the dissipation rate maximum (by around 40%), which is found with such methods to be closer to the blade than the present results indicated. The average integral length scale determined by the LDA data in the vicinity of ε_{max} was around $0.05D$, about 50% of that normally assumed in dimensional-relation estimates of ε. The microlength scales in the same location were all around 0.62 mm ($\sim 0.002T$), whereas the Kolgomorov scales varied from 23 to 30 μm ($\sim 0.0001T$) across the measurement region.

In addition, most the terms involved in the kinetic energy balance equation were evaluated and a balance was attempted with the dissipation rate directly measured. Notwithstanding some terms having been obtained from PIV results and the pressure diffusion being estimated from similar work performed by Escudié,[31] the results indicate that an acceptable level of balance of $\overline{q^2}$ was obtained.

Finally, the work presented in this paper has provided useful insights and methodologies for future measurements of ε in stirred vessels with both LDA and other techniques. In view of the fact that PIV methods with inherent spatial resolution limitations (such as those arising from the comparatively large scattering particle dimensions around 10 μm, in relation to those of the dissipative scales, around 25 μm) can be at present used only in low-Re stirred flows, the present method can provide a useful means of precisely quantifying the dissipation rate. Further work is needed to quantify in detail the phase-resolved variation of ε in stirred tanks, and thus provide improved ε_{max} and ε_{min} values to aid the design of fluid mixing processes. Phase-resolved data would be useful as well to deduce accurately the contribution of the pressure diffusion terms (of the organized and turbulent motions) from the kinetic energy balance. Only the contribution of the organized pressure diffusion was considered because the turbulent pressure diffusion was assumed to be negligible by Escudié,[31] although this assumption could and should be confirmed. The results presented also offer very useful data for the validation of predictions of ε in stirred tanks that use either the k–ε or the Smagorinsky SGS turbulence models.

Notation

A = constant, Eq. 2
C = impeller clearance, m
D = impeller diameter, m
$E_i(k_j)$ = kinetic energy of the ith velocity component per wavenumber k_j, $m^3\ s^{-2}$
$f_i(\Delta x_k)$ = variable, Eq. 5, $m^2\ s^{-2}$
H = water height in vessel, m
K_{ijhk} = coefficients in Eqs. 10, 11, and 12
k_i = wavenumber in the ith direction, m^{-1}
l = diffusive scale, m
L = convective scale, m
N = impeller rotational speed, s^{-1}; number of gradients measured
P_o = impeller power number
$\overline{q^2}$ = sum of the squared rms of the three velocity components, $m^2\ s^{-2}$
r = radial direction distance, m
Re = Reynolds number
$R_{ij}(\Delta x_k)$ = correlation of the ith and jth velocity components in two points at a distance Δx_k in the kth direction
T = vessel diameter, m
t = blade thickness, m; arrival time, s
U_j = velocity component in the jth direction, m s^{-1}
$\bar{U}_j$ = mean velocity component in the jth direction, m s^{-1}
u_j = fluctuating velocity component in the jth direction, m s^{-1}
u_j = rms of the velocity component in the jth direction, m s^{-1}
V_{tip} = velocity of the tip of the blade, m s^{-1}
X_1, $X2$, $X3$ = Cartesian coordinate system, m
z = axial direction distance, m

Greek letters

Δx_j = displacement in the jth direction, m
Δx_{j0} = minimum displacement Δx_j included in the range of fitting, m
Δx_{jmax} = maximum displacement Δx_j included in the range of fitting, m
ε = kinetic energy viscous dissipation rate, $m^2\ s^{-3}$
$\bar{\varepsilon}$ = kinetic energy viscous dissipation rate averaged over the whole vessel, $m^2\ s^{-3}$
ε_{max} = maximum kinetic energy viscous dissipation rate, $m^2\ s^{-3}$
ε_{min} = minimum kinetic energy viscous dissipation rate, $m^2\ s^{-3}$
η = Kolgomorov length scale, m
θ = tangential direction, °
Λ_{ij} = integral length scale of the ith velocity component in the jth direction, m
λ_{ij} = Taylor microscale of the ith velocity component in the jth direction, m
μ = dynamic viscosity, kg $m^{-1}\ s^{-1}$
ν = kinematic viscosity, $m^2\ s^{-1}$
ρ = density, kg m^{-3}
φ = blade angle, ° ($\varphi = 0°$ in the middle of a reference blade)

Abbreviations

2D = two-dimensional
3D = three-dimensional
CFD = computational fluid dynamics
DNS = direct numerical simulation
LDA/LDV = laser Doppler anemometry/velocimetry
LES = large eddy simulation
PIV = particle image velocimetry
RANS = Reynolds-averaged Navier–Stokes
rms = root mean squared

Literature Cited

1. Zhou G, Kresta SM. Impact of tank geometry on the maximum turbulence energy dissipation rate for impellers. *AIChE J*. 1996;42:2476-2490.
2. Nienow AW. On impeller circulation and mixing effectiveness in the turbulent flow regime. *Chem Eng Sci*. 1997;52:2557-2565.
3. Alopaeus V, Koskinen J, Keskinen KI. Simulation of the population balances for liquid–liquid systems in a non-ideal stirred tank. Part 1. Description and qualitative validation of the model. *Chem Eng Sci*. 1999;54:5887-5899.
4. Davies JT. A physical interpretation of drop sizes in homogenizers and agitated tanks, including the dispersion of viscous oils. *Chem Eng Sci*. 1987;42:1671-1676.
5. Pacek AW, Chamsart S, Nienow AW, Bakker A. The influence of impeller type on mean drop size and drop size distribution in an agitated vessel. *Chem Eng Sci*. 1999;54:4211-4222.
6. Bourne JR, Yu SY. Investigation of micromixing in stirred tank reactors using parallel reactions. *Ind Chem Eng Res*. 1994;33:41-55.
7. Cutter LA. Flow and turbulence in a stirred tank. *AIChE J*. 1966;12:35-45.
8. Kresta SM, Wood PE. The flow field produced by a pitched blade turbine: Characterization of the turbulence and estimate of the dissipation rate. *Chem Eng Sci*. 1993;48:1761-1774.
9. Wu H, Patterson GK. Laser Doppler measurements of turbulent flow parameters in a stirred mixer. *Chem Eng Sci*. 1989;44:2207-2221.
10. Escudié R, Liné A. Experimental analysis of hydrodynamics in a radially agitated tank. *AIChE J*. 2003;49:585-603.
11. Sheng J, Meng H, Fox RO. A large eddy PIV method for turbulence dissipation rate estimation. *Chem Eng Sci*. 2000;55:4423-4434.
12. Hinze JO. *Turbulence*. 2nd Edition. New York, NY: McGraw-Hill; 1972.
13. Sharp KV, Adrian RJ. PIV study of small-scale flow structure around a Rushton turbine. *AIChE J*. 2001;47:766-778.
14. Michelet S. *Turbulence et Dissipation au Sein d'un Réacteur agité par une Turbine Rushton–Vélocimétrie Laser Doppler à Deux de Mesure*. PhD Thesis. Lorraine, France: L'Institut National Polytechnique de Lorraine; 1998.
15. Derksen J, van den Akker HEA. Large eddy simulations on the flow driven by a Rushton turbine. *AIChE J*. 1999;45:209-221.
16. Ng K, Yianneskis M. Observations on the distribution of energy dissipation in stirred vessels. *Trans IChemE A*. 2000;78:334-341.
17. Zhou G, Kresta SM. Distribution of energy between convective and

turbulent flow for three frequently used impellers. *Trans IChemE A*. 1996;74:379-389.
18. Baldi S. *Energy Dissipation Measurements in Stirred Vessels with Particle Image Velocimetry*. PhD Thesis. London, UK: King's College London, University of London; 2004.
19. Benedict LH, Gould RD. Understanding biases in the near field region of LDA two-point correlation measurements. *Exp Fluids*. 1999;26: 381-388.
20. Kang S, Patil B, Roy RP. Effects of coincidence window and measuring volume size on laser Doppler velocimetry measurement of turbulence. *Exp Fluids*. 2001;30:365-370.
21. Ducci A, Konstantinidis E, Balabani S, Yianneskis M. Direct measurement of the turbulent kinetic energy viscous dissipation rate behind a grid and a circular cylinder. Proc 11th Int Symp on Applications of Laser Techniques to Fluids Mechanics, Lisbon, Portugal, Paper 33.1; 2002.
22. Gan CL, Djenidi L, Antonia RA. Spanwise vorticity measurements in a turbulent boundary layer using LDV. Proc 8th Int Symp on Applications of Laser Techniques to Fluids Mechanics, Lisbon, Portugal, Paper 17.2; 1996.
23. Saarenrinne P, Piirto M, Eloranta H. Experiences of turbulence measurement with PIV. *Meas Sci Technol*. 2001;12:1904-1910.
24. Ducci A. *Direct Measurement of the Viscous Dissipation Rate of Turbulent Kinetic Energy in a Stirred Vessel with Two-Point LDA*. PhD Thesis. London, UK: King's College London, University of London; 2004.
25. Lee KC, Yianneskis M. Turbulence properties of the impeller stream of a Rushton turbine. *AIChE J*. 1998;44:13-24.
26. Yianneskis M, Popiolek Z, Whitelaw JH. An experimental study of the steady and unsteady flow characteristics of stirred reactors. *J Fluid Mech*. 1987;175:537-555.
27. Khan FR, Rielly CD, Hargrave, GK. A multi-block approach to obtain angle-resolved PIV measurements of the mean flow and turbulence fields in a stirred vessels. Proc 11th Eur Conf on Mixing, Bamberg, Germany; 2003;47-54.
28. Yianneskis M, Whitelaw JH. On the structure of the trailing vortices around a Rushton turbine blades. *Trans IChemE*. 1993;71:543-550.
29. Lee KC. *An Experimental Investigation of the Trailing Vortex Structure and Mixing Characteristics of Mixing Vessels*. PhD Thesis. London, UK: King's College London, University of London; 1995.
30. Yeoh S. *Large Eddy Simulation of Turbulent Flow and Mixing Characteristics in a Stirred Vessel*. PhD Thesis. London, UK: King's College London, University of London; 2004.
31. Escudié R. *Structure locale de l'Hydrodynamique générée par une Turbine Rushton*. PhD Thesis. Toulouse, France: Institute National des Sciences Appliquées de Toulouse; 2001.
32. Derksen JJ, Doelman MS, van den Akker HEA. Three-dimensional LDA measurements in the impeller region of a turbulently stirred tank. *Exp Fluids*. 1999;27:522-532.

Manuscript received Jan. 16, 2004, and revision received Nov. 11, 2004.